PCCP

ROYAL SOCIETY OF CHEMISTRY

PAPER

View Article Online
View Journal | View Issue

Cite this: *Phys. Chem. Chem. Phys.*, 2024, **26**, 29121

A comprehensive guide for accurate conformational energies of microsolvated Li^+ clusters with organic carbonates†

Arseniy A. Otlyotov, [a] Andrey D. Moshchenkov,[a] Timofey P. Rozov,[ab] Anna A. Tuma,[ab] Alexander S. Ryzhako[ac] and Yury Minenkov *[a]

Organic carbonates and their mixtures are frequently used in electrolyte solutions in lithium-ion batteries. Rationalization and tuning of the related Li^+ solvation processes are rooted in the proper identification of the representative low-energy spatial structures of the microsolvated $Li^+(S)_n$ clusters. In this study, we introduce an automatically generated database of conformational energies (CEs), LICARBCONF806, comprising 806 diverse conformers of Li^+ clusters with 7 common organic carbonates. A number of standard and composite density functional theory (DFT) approaches and fast semi-empirical methods are examined to reproduce the reference CEs obtained at the RI-SCS-MP2/CBS level of theory. A hybrid PBE0-D4 functional paired with the def2-QZVP basis set is the most robust in reproducing the reference values while composite B97-3c demonstrates the best cost-benefit ratio. Contemporary tight-binding semi-empirical methods GFNn-xTB can be used for the filtering of high-energy structures, but their performance worsens significantly when the limited number of low-energy (CE $<$ 3 kcal mol^{-1}) conformers are to be sorted. Thermal corrections used to convert electronic energies to respective Gibbs free energies and especially corrections imposed by a continuum solvation model can significantly influence both the conformer ranking and the width of the CE distribution. These should be appropriately taken into account to identify lowest energy conformers in solution and at non-zero temperatures. The almost black-box conformation generation workflow used in this work successfully predicts representitative low-energy four-coordinated conformers of Li^+ clusters with cyclic carbonates and unravels the complex conformational nature of the clusters with flexible linear carbonates.

Received 6th September 2024,
Accepted 7th November 2024

DOI: 10.1039/d4cp03487b

rsc.li/pccp

1. Introduction

Organic carbonates and their mixtures have been long recognized as indispensable components of the electrolytes in lithium-ion batteries (LIBs).[1–6] Among the key properties of the carbonate electrolytes, their high Li^+ solvating power should be particularly noted.[5,7] According to the generally accepted concept, the solvation sheath is mainly assembled *via* the ion–dipole interactions between Li^+ and solvent molecules.[2] Unraveling of the solvation structures of Li^+ ion not only satisfies fundamental scientific curiosity, but also stimulates the development of high-performance electrolytes for the commercial LIBs.[8] Besides, representative structures of the most stable microsolvated $Li^+(S)_n$ clusters are needed for the reliable modeling of the ion solvation processes with use of the computational chemistry approaches. In particular, these species are involved in thermodynamic cycles for computation of the Li^+ ion solvation free energy within the framework of the cluster-continuum approach.[9,10]

Numerous recent experimental[11–19] and theoretical[20–26] studies of the Li^+ solvation shell structure were mainly focused on the coordination preference of either cyclic or linear carbonates and determination of the respective coordination numbers. However, relatively little attention has been paid to

[a] *N.N. Semenov Federal Research Center for Chemical Physics RAS, Kosygina Street 4, 119991 Moscow, Russia. E-mail: Yury.Minenkov@chph.ras.ru*
[b] *Department of Chemistry, Lomonosov Moscow State University, Leninskie Gory 1, Bld. 3, 119991 Moscow, Russia*
[c] *Dmitry Mendeleev University of Chemical Technology of Russia, Miusskaya sq. 9, 125047, Russia*

† Electronic supplementary information (ESI) available: ESI_PCCP_2024-11-07.pdf file contains numbers of conformers, maximum and average conformational energies, Pearson correlation coefficients and mean unsigned errors (MUEs) for the individual $Li^+(S)_n$ clusters, total times required for 1 SCF iteration (Tables S1–S8), lowest-energy conformers of $Li^+(S)_n$ clusters and flexible organic carbonates (Fig. S4–S43). ESI_PCCP.zip file includes Cartesian coordinates of conformers, additional computational data (total electronic energies by different DFT methods and SQM heats of formation, dipole moments, HOMO and LUMO energies, Hirshfeld and CM5 atomic charges, thermostatistical corrections according to (m)sRRHO models) and additional statistical data. See DOI: https://doi.org/10.1039/d4cp03487b

the conformational diversity of the $Li^+(S)_n$ species.[27,28] On the other hand, the overall reliability of theoretically predicted thermochemical characteristics of Li^+ solvation such as enthalpy (ΔH_{sol}), entropy (ΔS_{sol}) and free energy (ΔG_{sol}) is rooted in the appropriately determined low-energy spatial structures of $Li^+(S)_n$ clusters. Our recent experience in theoretical prediction of Na^+ solvation free energies[29–32] suggests that preliminary conformational sampling is a very time-consuming procedure and could even become a 'bottleneck' of the entire computational workflow. Three main current challenges can be distinguished. First, the large number of degrees of freedom associated with the relative spatial orientation of solvent molecules with respect to each other and Li^+ ion and their possible inherent conformational flexibility gives rise to a practically incalculable number of different conformations, especially in the case of larger coordination numbers ($n > 4$). Second, an affordable electronic structure theory method with a suitable cost-benefit ratio should be chosen for the screening of the relative conformational energies (CEs). Our recent study[30] on the CEs of $Na^+(S)_n$ clusters with some common protic and aprotic solvents revealed dispersion-corrected hybrid density functionals paired with triple-ζ quality basis sets to be the best performers, which is in line with the current state of the art in the field.[33] However, such calculations are expensive and usually become affordable only in the final stages of the conformational search, when the number of considered conformations is reduced to a few dozen species. Therefore, fast yet relatively accurate electronic structure theory methods for the intermediate stages of the conformational search are still to be established and validated on the specific systems under consideration. Finally, as practically important physico-chemical processes involving $Li^+(S)_n$ clusters occur at non-zero temperatures and in the presence of the bulk solvent, the influence of the corresponding thermal and solvent corrections on the conformational electronic energies should be taken into account for appropriate conformer ranking.

In the present contribution, we attempt to address all the above-mentioned issues considering CEs of $Li^+(S)_n$ clusters, where S is either a cyclic (CC) or a linear (LC) organic carbonate and the number n of the explicit solvent molecules ranges from 2 to 6. The following common carbonates were selected: propylene carbonate (PC), vinylene carbonate (VC), ethylene carbonate (EC), ethyl methyl carbonate (EMC), dimethyl carbonate (DMC), diethyl carbonate (DEC), and 1,2-butylene carbonate (BC). These specific cyclic (VC, EC, PC, BC) and linear (DMC, EMC, DEC) carbonates were chosen due to their relevance as ingredients of electrolytes in LIBs.[2,3,34,35] The development version of the Uniconf program recently created in our group was used for the automatic generation of diverse spatial structures of $Li^+(S)_n$ species forming the basis of the new conformational energy database termed LICARBCONF806. The performance of semi-empirical quantum mechanical methods (SQM) and contemporary (composite) density functional theory (DFT) approaches is examined against reference *ab initio* spin-component scaled RI-SCS-MP2 approximation. The impact of different models for Gibbs free energy thermodynamic corrections, including a modified scaled rigid rotor-harmonic oscillator (msRRHO) approach of Grimme[36,37] and its version extended for the vibrational enthalpy contribution[38] on the CEs is studied. Besides, we explore the influence of the conductor-like polarizable continuum model (PCM)[39–41] and recently developed in our group Solv model,[42] capturing non-electrostatic contributions to solvation free energy, on the relative energies of the conformations of $Li^+(S)_n$ clusters.

2. Computational details

2.1. Generation of initial conformations of Li^+ clusters with organic carbonates

The working version of the Uniconf program which is currently under active development in our group was used for the preliminary generation of spatially diverse structures of $Li^+(S)_n$ clusters. First, Li^+ ion and separate solvent molecules were randomly placed in space. Second, a set of variables was assigned to each solvent molecule, including 3 translational degrees of freedom for the center of mass, 3 rotational degrees of freedom corresponding to the rotations of a molecule about its principal axes of inertia and number of rotatable bonds (N_{rot} = 1 for BC, 2 for DMC, 3 for EMC and 4 for DEC). In total, $n(6 + N_{rot})$ variables were specified for each cluster and their values were optimized using the universal force field (UFF)[43] van der Waals and electrostatic energy terms to resolve possible inter- and intra-fragment steric clashes. All geometry parameters of the solvent molecules, except for the torsions along rotatable bonds were kept frozen at their starting values. In contrast to the various conformer generation strategies including intermediate structure optimizations with SQM methods (*e.g.* default GFN2-xTB[44] method in the CREST[45,46] program), this approach prevents possible artificial distortions of molecular structures and allows us to obtain both diverse and reasonable conformers without being tied to a particular PES of the questionable quality. The duplicates were ruled out[47–49] before and after the subsequent geometry optimization (Section 2.2) and up to 34 spatially diverse conformations of each cluster were subjected to the further processing.

2.2. Geometry optimization, calculation of vibrational frequencies and thermochemistry

Spatial structures of the conformations generated as described in the previous section were optimized using the PBE[50,51] functional complemented by D3(BJ)[52,53] empirical dispersion correction and paired with the def2-SVP basis set.[54] Auxiliary Coulomb fitting def2/J basis sets[55] were utilized as required in the resolution of the identity (RI) approximation.[56–58] The following tighter-than-default settings were specified: large DFT integration grid (DEFGRID3) and convergence tolerances TolE = 1×10^{-6} a.u., TolRMSG = 3×10^{-5} a.u., and TolMaxG = 1×10^{-4} a.u.

Harmonic vibrational frequencies were calculated for all optimized structures and checked for the absence of imaginary

modes. All quantum-chemical calculations were performed using the ORCA 5.0.4 program.[59–61]

Thermochemical corrections needed to convert total electronic energies to Gibbs free energies were computed within the scaled rigid rotor-harmonic oscillator (sRRHO) approximation. All frequencies were scaled by a factor of 1.011 as suggested in ref. 62 for PBE/6-31G(d) model chemistry. We also employed a modified version of the sRRHO approach (msRRHO) proposed by Grimme[36,37] in order to prevent vibrational contribution to molecular entropy (S_{vib}) from being spoiled by low vibrational frequencies which are typical for the considered $Li^+(S)_n$ species. Additionally, we utilized a recently suggested expanded version of the msRRHO approach,[38] which corrects the vibrational contribution to the enthalpy (H_{vib}) along with the original modification of S_{vib}. In both variants the cut-off frequency τ = 100 cm^{-1} and parameter α = 4 were used. Further in this paper, we will denote the original msRRHO implementation, where only S_{vib} is corrected, as msRRHO(100,4,0) and its expanded version as msRRHO(100,4,1).

2.3. Methods for the evaluation of single-point energies

Reference conformational energies were obtained with spin-component scaled RI-SCS-MP2 approximation.[63] All-electron Karlsruhe basis sets def2-nZVPP (n = T, Q)[54] were utilized with further complete basis set (CBS) extrapolation with the use of the well-tested[64,65] $1/(l_{max} + 1/2)^4$ scheme of Martin.[66] The auxiliary correlation fitting def2-nZVPP/C[67] basis sets were employed.

The performance of the common *meta*-generalized-gradient approximation (*m*GGA) r^2SCAN[68,69] and hybrid (B3LYP[70–72] and PBE0[73]) functionals complemented by D4[74,75] dispersion correction along with the range-separated hybrid *meta*-GGA ωB97M-V[76] functional with VV10[77] correction (invoked in the default post-SCF way[78]) was assessed. For these calculations, def2-nZVP (n = T, Q)[54] basis sets were employed and CBS extrapolation was carried out as described above. Later in the text def2-nZVP (and def2-nZVPP for the RI-SCS-MP2 method) basis sets are referred to as TZ (for n = T) and QZ (for n = Q).

Besides, single-point energies (SPEs) of the PBE-D3(BJ)/def2-SVP optimized structures (Section 2.2) were also used in the statistical analysis. In addition, SPEs were obtained with the contemporary composite DFT approaches, PBEh-3c,[79] B97-3c[80] and r^2-SCAN-3c.[81]

As a low-cost alternative for the DFT methods, a number of SQM approximations were tested, including neglect of diatomic differential overlap (NDDO) based AM1,[82] PM3,[83] PM6,[84] PM6-D3,[52,84] PM6-D3H4[84,85] and PM7,[86] contemporary tight-binding GFN*n*-*x*TB (n = 1, 2)[44,87] and also the NDDO-like method by Laikov[88,89] (hereinafter referred to as QM3) developed to reproduce CCSD(T) data and requested *via* qm_n3 keyword in the Priroda program.[90] These calculations were performed using MOPAC2016,[91] xtb 6.7.0[92] and Priroda[90] computer codes. In all MOPAC calculations the PRECISE keyword was specified for the sake of accuracy.

2.4. Correction of conformational energies due to an implicit solvent model

Several continuum solvation models were used to study the influence of the implicit solvation on the CEs. First, the performance of the common PCM model was examined. Additional [PCM] ωB97M-V/def2-TZVP SPE calculations were performed and final SPEs in the presence of the implicit solvent (E_{Solv}) were approximated as:

$$E_{Solv} = E(\text{RI-SCS-MP2/CBS}) + (E([\text{PCM}]\ \omega\text{B97M-V/TZ}) - E(\omega\text{B97M-V/TZ})) \quad (1)$$

Second, the Solv model,[42] recently developed in our group, combining non-iterative COSMO[93] solvation energies and non-electrostatic terms was employed and the respective E_{Solv} values were calculated as:

$$E_{Solv} = E(\text{RI-SCS-MP2/CBS}) + \Delta G_{Solv} \quad (2)$$

where ΔG_{Solv} contribution was obtained using the Solv program within the scaled particle theory-volume (SPT-V) formalism. The calculations were performed with CM5 charges[94] computed[95,96] from Hirshfeld atomic charges obtained at the ωB97M-V/def2-TZVP level of theory.

2.5. Statistical measures

The conformational rankings according to different methods were compared for each particular $Li^+(S)_n$ cluster in terms of the Pearson correlation coefficient:

$$\rho(X,Y) = \frac{\sum_{i=1}^{N}\left(E_{x,i} - \overline{E_x}\right)\left(E_{y,i} - \overline{E_y}\right)}{\sqrt{\sum_{i=1}^{N}\left(E_{x,i} - \overline{E_x}\right)^2 \sum_{i=1}^{N}\left(E_{y,i} - \overline{E_y}\right)^2}}, \quad (3)$$

where X is the examined electronic structure approach, Y is the reference method (RI-SCS-MP2/CBS, unless otherwise noted), E_i are the relative conformational energies, $\bar{E}$ are the average conformational energies for a given method, and N is the number of conformations for a $Li^+(S)_n$ cluster. Positive and close to 1.0 values reflect a strong correlation between the tested methods, while negative ρ close to −1.0 correspond to anti-correlation.

Quantitative differences in conformational energies predicted by different methods are expressed by mean signed and mean unsigned errors (MSEs and MUEs):

$$\text{MUE}(X,Y) = \frac{\sum_{i=1}^{N}|E_i(X) - E_i(Y)|}{N} \quad (4)$$

$$\text{MSE}(X,Y) = \frac{\sum_{i=1}^{N}(E_i(X) - E_i(Y))}{N} \quad (5)$$

where X and Y are the examined and reference electronic structure methods, N is the number of conformations for a $Li^+(S)_n$ cluster, and E_i are the relative conformational energies.

Statistical analysis was performed only for the clusters for which at least 10 diverse conformations were obtained. According to the chosen threshold, the clusters $Li^+(DMC)_2$, $Li^+(EC)_2$, $Li^+(EC)_3$, $Li^+(PC)_2$, $Li^+(VC)_2$, and $Li^+(VC)_3$ were discarded.

3. Results and discussion

3.1. Impact of a quantum-chemical approximation on the conformational energies

3.1.1. Effect of the CBS extrapolation on the conformational energies. DFT functionals paired with at least triple-ζ quality basis sets represent a well-established combination for accurate CEs provided a sufficiently dense integration grid.[33] In this work, we also performed SPE calculations with quadruple-ζ basis sets followed by CBS extrapolation. Comparison of the CEs obtained with the same method (MP2, B3LYP-D4, PBE0-D4, r^{2}SCAN-D4 and ωB97M-V) and different basis sets (TZ and QZ) indicates their excellent correlation with the CBS-based values with all median Pearson coefficients of 1.0. Median MUEs between QZ and CBS CEs are *ca.* 0.1 kcal mol^{-1} indicating QZ quality basis sets to be sufficient for their evaluation without CBS extrapolation, see Fig. S1 in the ESI† for details. Larger MUEs of 0.2 kcal mol^{-1} were obtained for TZ energies computed with DFT methods while in the case of the *ab initio* RI-SCS-MP2 method the median MUE reaches 0.4 kcal mol^{-1} reflecting slower convergence to the CBS limit. The maximum MUE between CBS and TZ CEs is 0.7 kcal mol^{-1} for both MP2 and DFT methods. These numerical results show that while TZ CEs are sufficient for the conformer ranking, non-negligible maximum MUEs imply that predicted Boltzmann populations may be largely shifted. Further in the text only CBS extrapolated CEs will be discussed in the case of RI-SCS-MP2 and standard DFT methods, unless otherwise noted.

3.1.2. Conformational energies from standard and composite DFT methods. Standard DFT approximations (B3LYP-D4, PBE0-D4, r^{2}SCAN-D4 and ωB97M-V) yield CEs exhibiting excellent correlation (median ρ = 0.99) with the respective RI-SCS-MP2 values (Fig. 1). In the case of B3LYP-D4, r^{2}SCAN-D4 and ωB97M-V

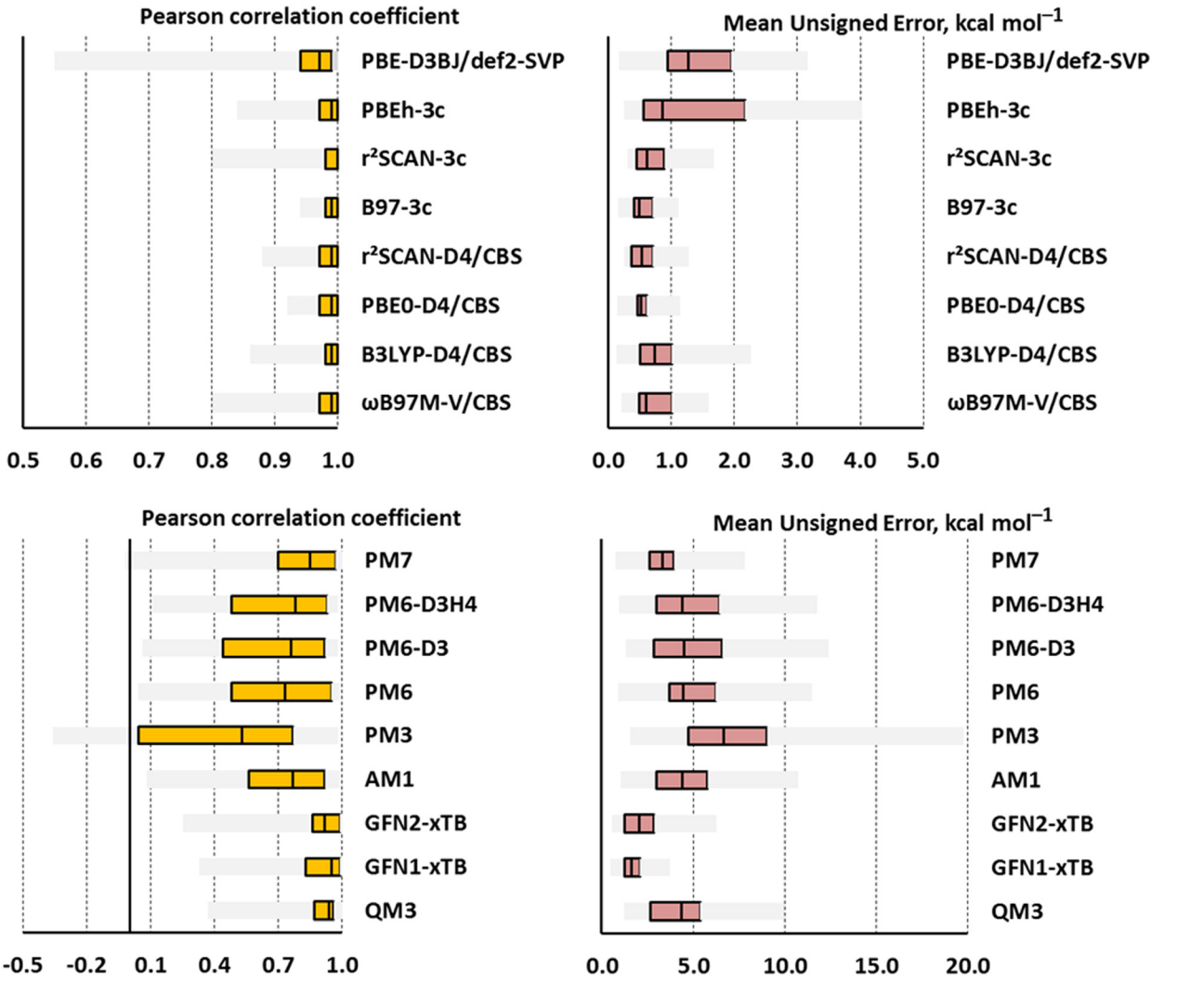

Fig. 1 Pearson correlation coefficients and mean unsigned errors (MUEs) for the DFT and SQM considered in this work with respect to the reference RI-SCS-MP2/CBS approximation. The left/right sides of the rectangles correspond to the first (Q_1) and third (Q_3) quartiles, respectively. The vertical bold line inside each rectangle shows the median value. The left/right sides of the gray boxes display the lowest/largest values for each method. Detailed statistics for all $Li^+(S)_n$ clusters are given in Tables S1–S4 (ESI†).

functionals the lowest ρ values were found for the $Li^+(BC)_4$ system with the narrowest CE span (CE_{max} = 2.6 kcal mol^{-1}, CE_{avg} = 1.6 kcal mol^{-1}).

Assuming the energy window of the conformers populated at room temperature is 3 kcal mol^{-1}, we additionally calculated statistical measures for the reduced ensembles of the clusters forming the LICARBCONF806 database containing 308 conformations of 21 $Li^+(S)_n$ clusters with CE(RI-SCS-MP2) $<$ 3 kcal mol^{-1}. For these reduced ensembles hereinafter referred to as LICARBCONF308, lower ρ values ranging from 0.91 (ωB97M-V) to 0.96 (PBE0-D4) and wider inter-quartile ranges (IQRs = $Q_3 - Q_1$) of 0.05–0.16 were obtained, see Fig. S2 in the ESI.†

In terms of the mean unsigned errors calculated for the entire LICARBCONF806 database, PBE0-D4 CEs are the closest to the reference RI-SCS-MP2 counterparts (MUE = 0.5 kcal mol^{-1}) followed by r^{2}SCAN values with a slightly wider IQR, see Fig. 1. CEs from the B3LYP-D4 and ωB97M-V functionals are in worse agreement with the reference CEs with MUEs of *ca.* 0.8 kcal mol^{-1}. The smallest MUE of 0.3 kcal mol^{-1} was also found for PBE0-D4 CEs computed for the LICARBCONF308 set.

Turning to the composite DFT approaches (B97-3c, r^{2}SCAN-3c and PBEh-3c), we should mention that their statistical characteristics are similar to those yielded for standard DFT functionals. The worse performance of the PBEh-3c method (based on def2-mSVP basis set, MUE_{avg} = 1.4 kcal mol^{-1}) and also the PBE-D3(BJ)/def2-SVP approximation (MUE_{avg} = 1.5 kcal mol^{-1}) used for geometry optimization supports the well-known insufficiency of the DZ basis sets for accurate CEs. However, it should be noted that PBEh-3c performs equally with the other composite approaches on the reduced LICARBCONF308 set.

The computational efficiency of the considered DFT methods was evaluated by comparison of the relative times required for 1 SCF iteration (Fig. 2). The most robust in reproducing reference CEs, the PBE0-D4 method is 3 to 5 times more expensive compared to the composite B97-3c. Therefore, the latter method can be a cheaper alternative in the case of the limited computational resources.

3.1.3. Conformational energies from semi-empirical methods. Semi-empirical methods (SQM) are commonly used at the initial stages of the multi-level strategies of conformational analysis. For this reason, their ability for at least qualitative filtering of the low-energy conformers is critical to save as many as possible of them for further treatment with higher-level methods. Classical SQM approaches, AM1 and different variants of the parametric method (PM), exhibit poor performance in predicting CEs of the LICARBCONF806 set. The Pearson coefficient IQRs calculated for these methods are in the range of 0.3–0.7, which is about 10 times wider compared to the DFT approximations, see Fig. 1. Large deviations of the CEs from the reference RI-SCS-MP2 values are not systematic as reflected by vanishing MSEs, not exceeding 0.4 kcal mol^{-1} (the only exception is PM3 with MSE = 4.9 kcal mol^{-1}), while the corresponding MUEs are in the range of 3.5–7.2 kcal mol^{-1}. Contemporary tight-binding GFN*n*-xTB methods yield CEs which demonstrate good correlation with the reference values. In line with our previous study of CEs of Na^+ with protic and aprotic solvents,[30] more recent GFN2-xTB is not superior to its GFN1-xTB predecessor as it stems from the respective median correlation coefficient of 0.92 and 0.95 as well as MUEs of 2.5 and 1.7 kcal mol^{-1}. Despite overall good performance, particular $Li^+(S)_n$ species suddenly turned out to be challenging for these methods. For example, only weak correlation with the

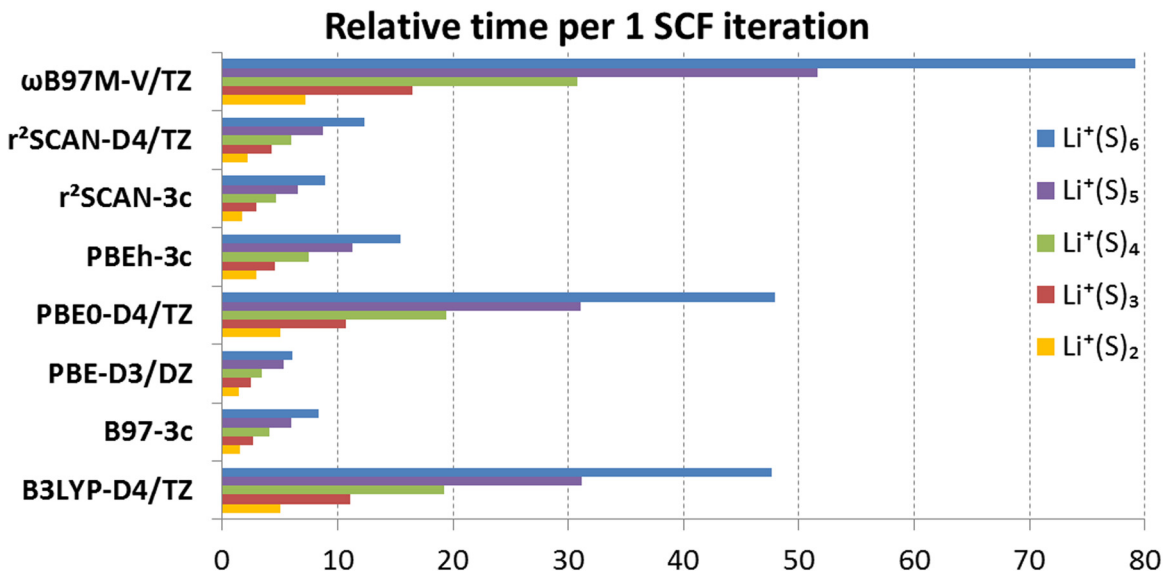

Fig. 2 Relative time per 1 SCF iteration for standard and composite DFT methods and $Li^+(S)_n$ clusters with n = 2–6. The values are averaged over all the considered solvents and related to the smallest time of t_{min} = 3.3 s for $Li^+(VC)_2$ at the PBE-D3(BJ)/def2-SVP level of theory obtained on a 16-core AMD Ryzen 9 5950X processor. Absolute times are given in Table S5 (ESI†).

reference CEs was found for the $Li^+(DEC)_6$ cluster (ρ_{GFN1} = 0.33, ρ_{GFN2} = 0.25). Even more importantly, median correlation coefficients for both GFN*n*-xTB methods drop dramatically (ρ_{GFN1} = 0.43, ρ_{GFN2} = 0.48) if only low-energy conformers constituting the LICARBCONF308 subset are considered, see Fig. S2 in the ESI.† Therefore, while these fast SQM approaches can be used to rule out high energy conformations of $Li^+(S)_n$ clusters within the larger energy scales, they should be used with caution if proper ranking of the low energy (<3 kcal mol^{-1}) conformers is required. The QM3 method implemented in the Priroda program demonstrates a more promising performance in the conformer ranking for the considered species compared to the other SQM approaches as the correlation coefficient only reduces from 0.94 to 0.79 for the low-energy LICARBCONF308 subset, but exhibits large absolute deviations in CEs with an average MUE of 4.6 kcal mol^{-1} as calculated for the main LICARBCONF806 set.

3.2. Impact of the vibrational thermochemistry and continuum solvation models on conformational energies

In this section we discuss the influence of the thermal correction to Gibbs free energy (ΔG_{corr}) and correction accounting for the presence of the continuum solvent (ΔG_{Solv}) on the CEs. The cumulative effect of both corrections is also considered for all conformers as well as for a smaller subset of the low-energy species, see Fig. 3 and Fig. S3 in the ESI,† respectively. First, standard sRRHO approximation may completely change the conformer ranking in the case of extremely low frequencies due to their large impact on the vibrational entropy (S_{vib}). For example, weak correlation (ρ_{sRRHO} = 0.20) with the reference RI-SCS-MP2 conformational electronic energies was found for the $Li^+(EC)_6$ cluster. In the case of this system the second highest energy conformer with CE(RI-SCS-MP2) = 15.2 kcal mol^{-1} turns out to be the lowest energy one if CEs including ΔG_{corr}(sRRHO) are compared illustrating the huge impact of nine low frequencies in the range of 0.8–9.5 cm^{-1} for this particular structure. The modified sRRHO method (msRRHO) increases the robustness of CEs in the presence of abundant low frequencies, *i.e.* CEs obtained with ΔG_{corr} from msRRHO methods correlate better with their reference RI-SCS-MP2 counterparts compared to CEs including ΔG_{corr}(sRRHO) corrections. A close performance with median ρ = 0.99 and mean MUE of 0.2 kcal mol^{-1} was found for the original msRRHO method[36,37] and its recently proposed version expanded for the vibrational contribution to enthalpy.[38] The former model termed msRRHO(100,4,0) yielded CEs slightly closer to their non-corrected RI-SCS-MP2 counterparts. However, for some species the lowest Gibbs free energy structures are higher-energy conformers according to the reference RI-SCS-MP2 electronic energies. For example, in the case of $Li^+(DMC)_6$, the lowest energy structure according to both variants of the msRRHO approach, is 3.1 $kcal^{-1}$ higher in energy compared to the RI-SCS-MP2 CEs. Analysis of Fig. 4 suggests that thermostatistical Gibbs free energy corrections do in most cases not affect the width of the CEs distribution (median $\Delta E_{max}/\Delta G_{max}$ = 0.9–1.0). In other words, maximum and mean CEs are close to their reference analogues.

Continuum solvation models exhibit a larger influence on CEs. Median correlation coefficients remain sufficiently large (ρ_{PCM} = 0.93 and ρ_{Solv} = 0.97), but IQRs are wider compared to that for the different thermochemistry models. Furthermore, the maximum values of CEs in the solvent (ΔG_{max}) become on average 30–40% smaller compared to the reference CEs in the gas phase (see Fig. 4). While the lowest energy conformers predicted using solvation free energies from the Solv program are generally similar to their reference counterparts, the PCM model which captures only electrostatic contributions to ΔG_{Solv} can in some cases significantly reduce CE stabilizing a highly unfavorable gas-phase conformer in solution. For example, the low energy conformers of $Li^+(BC)_5$ (CE_{PCM} = 0), $Li^+(EC)_5$ (CE_{PCM} = 0.8 kcal mol^{-1}) and $Li^+(PC)_6$ (CE_{PCM} = 0.2 kcal mol^{-1}), obtained with the PCM model turn out to be unfavorable by more than 5 kcal mol^{-1} according to the reference CEs.

Simultaneous application of both thermostatistical (ΔG_{corr}) and continuum solvation (ΔG_{Solv}) substantially lowers the

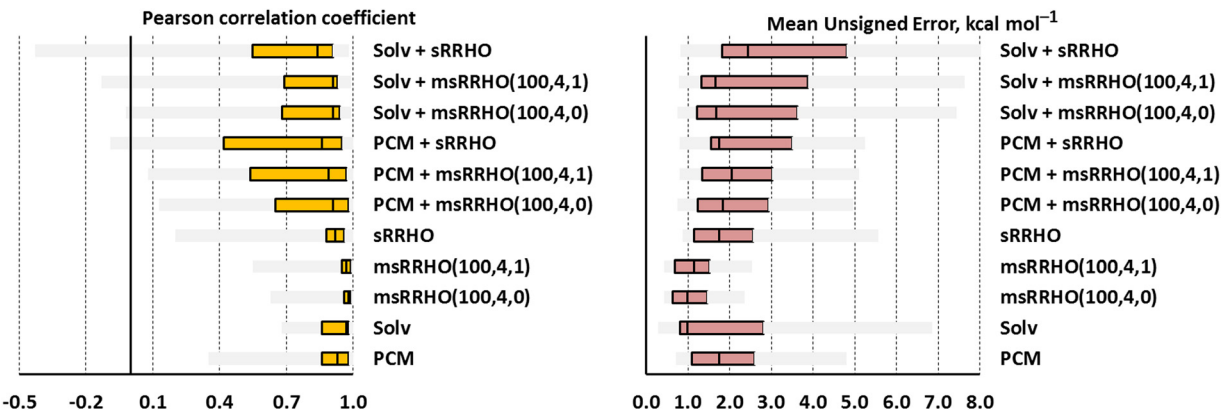

Fig. 3 Pearson correlation coefficients and mean unsigned errors (MUEs) for the different models for vibrational thermostatistical corrections (sRRHO and msRRHO) and continuum solvation models (PCM and Solv). Both statistical measures are computed *versus* reference gas-phase RI-SCS-MP2/CBS conformational energies. A description of the models is given in Section 2.4. The left/right sides of the rectangles correspond to the first (Q_1) and third (Q_3) quartiles, respectively. The vertical bold line inside each rectangle shows the median value. The left/right sides of the gray boxes display the lowest/largest values for each method. Detailed statistics for all $Li^+(S)_n$ clusters are given in Tables S6 and S7 (ESI†).

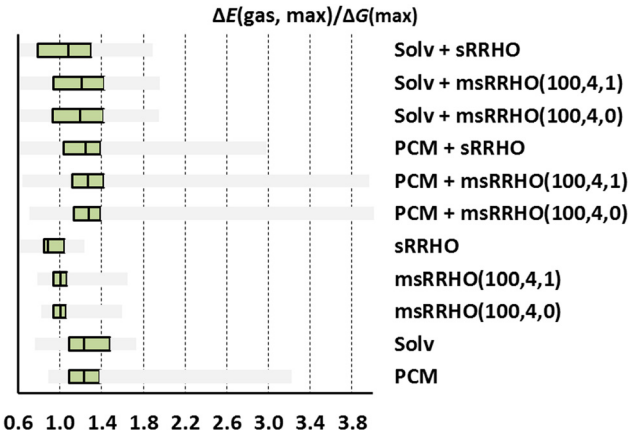

Fig. 4 Impact of vibrational thermostatistical corrections (sRRHO and msRRHO) and continuum solvation models (PCM and Solv) on the conformational energy span. Maximum conformational electronic energies ($\Delta E_{gas,max}$) are computed at the RI-SCS-MP2/CBS level of theory. The left/right sides of the rectangles correspond to the first (Q_1) and third (Q_3) quartiles, respectively. The vertical bold line inside each rectangle shows the median value. The left/right sides of the gray boxes display the lowest/largest values for each method. Absolute ΔE(gas, max) and ΔG(max) values are given in Table S8 (ESI†).

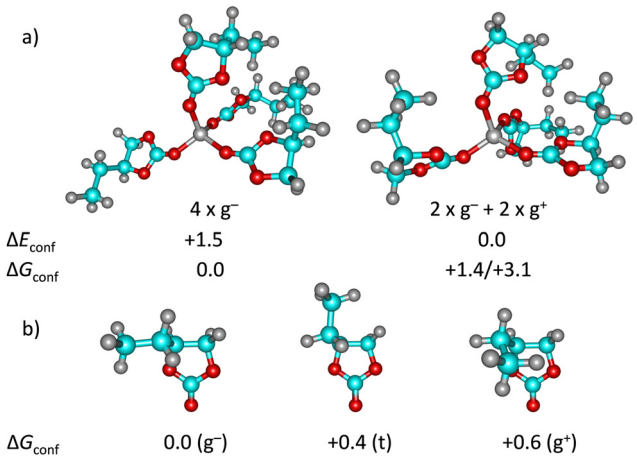

Fig. 5 Lowest electronic (ΔE_{conf}) and Gibbs free energy (ΔG_{conf}) spatial structures of the $Li^+(BC)_4$ cluster (a) and 1,2-butylene carbonate, BC (b). Conformational energies are given in kcal mol^{-1}. The spread in ΔG_{conf} refers to the influence of a particular combination of the continuum solvation model (PCM or Solv) and thermostatistical correction (HO, msRRHO(100,4,0), msRRHO(100,4,1)). Atom color coding: carbon (turquoise), oxygen (red), hydrogen (gray), and lithium (gray).

correlation of the resulting conformational Gibbs energies with RI-SCS-MP2 conformational electronic energies for some $Li^+(S)_n$ species as can be visually observed by comparison of the IQRs (Fig. 3). The lowest energy conformers deviate significantly from their reference counterparts, especially in the case of the clusters with n = 5, 6.

3.3. Lowest energy spatial structures of Li^+ carbonates and their significance for accurate calculations of solvation free energies

The conformational ensembles of $Li^+(S)_n$ clusters were originally constructed (see Section 2.1) to cover the most spatially diverse structures which is essential to obtain a sufficiently large span of CEs. However, it is expected that some of the structures are representative low-energy conformations to be used for the modeling of the Li^+ ion solvation processes. To verify this hypothesis, we proceed to the visual assessment of the predicted conformers and compare them, where possible, with the previously derived experimental and theoretical molecular structures of the $Li^+(S)_n$ species. The most common coordination number n = 4 was chosen for all the considered organic carbonates.

3.3.1. Predicted structures of Li^+ clusters with cyclic carbonates. Cyclic carbonates (CCs) do not exhibit inherent conformational flexibility, except for BC, and the conformers of the $Li^+(CC)_4$ differ only by the arrangement of the solvent molecules around the Li^+ ion. For the clusters with VC, EC and PC their well-established conformers[16,23] with four carbonate molecules forming a tetrahedron around Li^+ ion were predicted (see Fig. S4–S6, ESI†). Note, that for $Li^+(VC)_4$ and $Li^+(PC)_4$, their lowest electronic (ΔE_{conf}) and Gibbs free energy (ΔG_{conf}) conformers differ by location of the carbonate molecules with respect to each other and the Li^+ ion. In the case of $Li^+(BC)_4$, the structure with the lowest Gibbs free energy (Fig. 5a, left) is composed only of the lowest energy *gauche* (g^-) conformers of BC (Fig. 5b). In contrast, the higher energy g^+ conformers contribute to the lowest electronic energy structure of $Li^+(BC)_4$ (Fig. 5a, right) along with the g^- ones. Visual inspection of the higher-energy conformers of $Li^+(CC)_4$ clusters expectedly suggests that their CEs gradually increase along with a decrease in the number of carbonate molecules bound directly to the Li^+ ion.

3.3.2. Predicted structures of Li^+ clusters with linear carbonates. A conformational search becomes significantly more challenging in the case of $Li^+(LC)_4$ clusters due to the complex conformational landscape of linear carbonates (LCs). The simplest canonical example is the $Li^+(DMC)_4$ cluster (Fig. 6) for which the presence of the energetically unfavourable *cis–trans* (*ct*) conformer of DMC (Fig. 6b) in the first solvation shell of Li^+ was confirmed in the previous experimental[97] and theoretical[16] studies. Similarly, the lowest energy conformer of $Li^+(DMC)_4$ predicted in this work contains three DMC molecules in a *ct* conformation and one DMC molecule in a *cis–cis* (*cc*) conformation (Fig. 6a, left). It is important to note that the lowest energy $Li^+(DMC)_4$ cluster composed exclusively of the lowest energy *cc* conformers of DMC turns out to be highly energetically unfavourable (Fig. 6a, right).

Linear carbonates with elongated alkyl chains possess a more rich conformational landscape. Using the Uniconf program in the systematic conformational search mode (see the ESI† for details), we identified six conformers of EMC and nine conformers of DEC. It should be noted that similar conformers of DEC were previously determined by Viswanathan and coworkers.[98] Further in the text the common notation describing *cis* (*c*), *trans* (*t*) and *gauche* ($g^{\pm}$) stereochemical arrangements will be used. For example, a conformer of EMC denoted as *ct*(*t*) (see Fig. S7b, ESI†) possesses two anomeric carbon atoms in *cis*

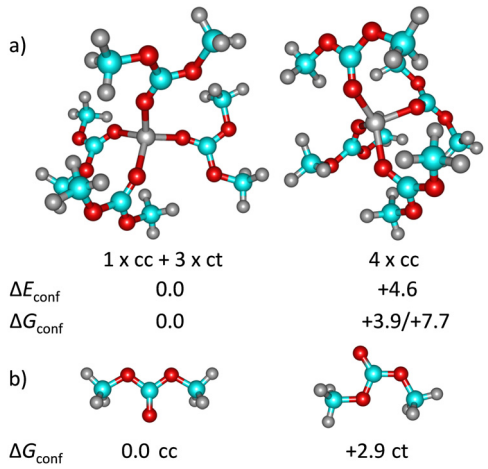

Fig. 6 Lowest electronic (ΔE_{conf}) and Gibbs free energy (ΔG_{conf}) and higher-energy spatial structures of the $Li^+(DMC)_4$ cluster (a) and *cis–cis* (*cc*) and *cis–trans* (*ct*) conformers of dimethyl carbonate, DMC (b). Conformational energies are given in kcal mol^{-1}. The spread in ΔG_{conf} for the high-energy $Li^+(DMC)_4$ cluster refers to the influence of a particular combination of the continuum solvation model (PCM or Solv) and thermostatistical correction (HO, msRRHO(100,4,0), msRRHO(100,4,1)). Atom color coding: carbon (turquoise), oxygen (red), hydrogen (gray), and lithium (gray).

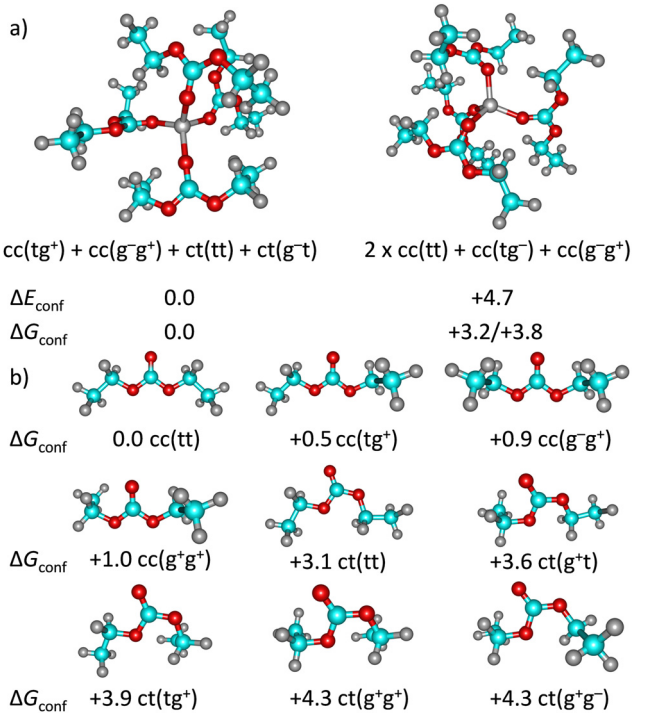

Fig. 7 Lowest electronic (ΔE_{conf}) and Gibbs free energy (ΔG_{conf}) and higher-energy spatial structures of the $Li^+(DEC)_4$ cluster (a) and conformers of diethyl carbonate, DEC (b). Conformational energies are given in kcal mol^{-1}. The spread in ΔG_{conf} for the high-energy $Li^+(DEC)_4$ cluster refers to the influence of a particular combination of the continuum solvation model (PCM or Solv) and thermostatistical correction (HO, msRRHO(100,4,0), msRRHO(100,4,1)). Atom color coding: carbon (turquoise), oxygen (red), hydrogen (gray), and lithium (gray).

and *trans* configurations with respect to the C═O moiety (dihedral angle C–O–C═O) and a terminal carbon atom (attached to the *trans* – anomeric carbon) in the *trans* configuration (dihedral angle C–C–O–C). Similarly to $Li^+(DMC)_4$ species, lowest energy spatial structures of $Li^+(EMC)_4$ clusters contain high energy *ct*(*t*) and *ct*($g^{\pm}$) conformers of EMC (Fig. S7a, ESI†).

Finally, the lowest energy structure of $Li^+(DEC)_4$ contains DEC molecules in four different conformations, again including unfavourable *ct* structures of DEC (see Fig. 7). At the same time, an arbitrary fine-looking structure (Fig. 7a, right) formed by energetically favourable *cis–cis* conformers of DEC possesses a significantly higher CE.

Overall, our inspection of the generated structures of $Li^+(LC)_4$ clusters clearly indicate that one can hardly rely on a chemical intuition and guess a low-energy conformer without a thorough conformational search taking into account both orientation of the solvent molecules around the central ion and their internal degrees of freedom. Finding a representative low-energy conformer of a $Li^+(S)_n$ cluster is critically important for the reliable predictions of solvation free energies in the framework of either monomer or cluster thermodynamic cycles of the cluster-continuum approach.[9,10] In this method, the error associated with an improperly chosen high energy conformer directly transfers into the error in the solvation free energy. We believe that along with the other conformational search strategies, the approach implemented in the Uniconf program may be of assistance to discover low-energy conformers of such systems in an almost black-box fashion.

4. Conclusions

Reliable identification of the low-energy conformers of microsolvated Li^+ clusters with organic carbonates is critically important for a deeper understanding of the solvation processes occurring in the electrolytes of Li-ion batteries. In this work, we introduce an automatically generated conformational energy database, LICARBCONF806, comprising 806 diverse conformers of the Li^+ ion with 7 common organic carbonates. A battery of contemporary density functional theory and fast semi-empirical approaches are examined to reproduce reference *ab initio* RI-SCS-MP2/CBS conformational energies of $Li^+(S)_n$ clusters. Using the hybrid PBE0 functional complemented by D4 empirical dispersion correction was found to be the most robust, while the composite B97-3c approach turned out to be the most efficient assuming the cost-benefit ratio. Classical semi-empirical methods, AM1 and different versions of the parametric method (PM), should be used with caution as the conformational energies can be largely and non-systematically shifted from their reference counterparts as reflected by relatively low Pearson correlation coefficients and mean signed errors which differ by sign for different $Li^+(S)_n$ clusters. Tight-binding GFN*n*-xTB approaches are clearly more promising at least for the filtering of high-energy structures, but their performance worsens significantly (mean ρ = 0.46) when the

limited number of low-energy (CE < 3 kcal mol^{-1}) conformers are to be sorted.

Thermostatistical corrections do not largely affect the width of the conformer energy distribution, but in cases of abundant and very low frequencies can alter the ranking of conformers. Expectedly, the modified scaled rigid-rotor-harmonic-oscillator (msRRHO) approach makes it more robust with respect to the applied ΔG_{corr} compared to the standard sRRHO approximation. In contrast, correction of the conformational energies for the presence of the continuum solvent (ΔG_{Solv}) narrows their range by 30–40% and in some cases leads to the stabilization of the conformers highly unfavorable in the gas phase. The correlation between reference RI-SCS-MP2/CBS conformational energies and their corrected analogues lowers when both corrections (ΔG_{corr} and ΔG_{Solv}) are applied simultaneously.

Visual assessment was performed for the lowest-energy conformers of Li(S)$_n$ clusters with the most common coordination number of $n = 4$. In the case of cyclic carbonates (VC, EC, PC) which do not exhibit inherent conformational flexibility, the well-established four-coordinated conformers of Li$^+$(CC)$_4$ were successfully determined. Inspection of the clusters with flexible carbonates (cyclic BC and linear DMC, EMC, DEC) indicated that their lowest-energy conformers do not necessarily originate from the lowest-energy conformers of the corresponding solvent molecules. We should note, that this conclusion supported by the previous experimental and theoretical studies, was obtained using an almost black-box computational workflow based on the Uniconf program and without using any insights from the earlier investigations.

Overall, the results of this study indicate the importance of appropriately accounting for the thermochemical and continuum solvation corrections, as they may both significantly affect the conformer ranking and in turn, the predicted lowest energy conformers. The developed LICARBCONF806 database can be used for the calibration of the emerging computationally efficient electronic structure methods and also provides representative low-energy conformers of the Li$^+$ ion in the most common organic carbonates.

Author contributions

The manuscript was written through contributions of all authors.

Data availability

The Uniconf program 64-bit Linux binary as well as the user's manual are available for download free of charge at **https://github.com/QuantumChemistryGroup/uniconf_binary/releases/tag/v1.0**. The thermochemistry code enabling both standard harmonic oscillator and msRRHO calculations is available for download free of charge at **https://github.com/QuantumChemistryGroup/thermochemistry**. The Python 3 scripts for conversion of the ORCA Hirshfeld charges to their CM5 counterparts are available free of charge at **https://github.com/QuantumChemistryGroup/orca2cm5/releases/tag/v1.0**. The Solv computer program is available for download free of charge at **https://github.com/QuantumChemistryGroup/solv/releases/tag/v1.0**.

Conflicts of interest

There are no conflicts to declare.

Acknowledgements

The work was financially supported by the Russian Science Foundation (project 24-23-00301). For computer time, this research used the resources of the Joint Supercomputer Center of RAS in Moscow, Russia. The anonymous reviewers of this work are gratefully acknowledged for their useful comments and suggestions.

Notes and references

1 K. Xu, Nonaqueous Liquid Electrolytes for Lithium-Based Rechargeable Batteries, *Chem. Rev.*, 2004, **104**, 4303–4418.
2 K. Xu, Electrolytes and Interphases in Li-Ion Batteries and Beyond, *Chem. Rev.*, 2014, **114**, 11503–11618.
3 J. Kalhoff, G. G. Eshetu, D. Bresser and S. Passerini, Safer Electrolytes for Lithium-Ion Batteries: State of the Art and Perspectives, *ChemSusChem*, 2015, **8**, 2154–2175.
4 B. Flamme, G. Rodriguez Garcia, M. Weil, M. Haddad, P. Phansavath, V. Ratovelomanana-Vidal and A. Chagnes, Guidelines to design organic electrolytes for lithium-ion batteries: environmental impact, physicochemical and electrochemical properties, *Green Chem.*, 2017, **19**, 1828–1849.
5 C.-C. Su, M. He, R. Amine, T. Rojas, L. Cheng, A. T. Ngo and K. Amine, Solvating power series of electrolyte solvents for lithium batteries, *Energy Environ. Sci.*, 2019, **12**, 1249–1254.
6 M. Li, C. Wang, Z. Chen, K. Xu and J. Lu, New Concepts in Electrolytes, *Chem. Rev.*, 2020, **120**, 6783–6819.
7 K. Chen, X. Shen, L. Luo, H. Chen, R. Cao, X. Feng, W. Chen, Y. Fang and Y. Cao, Correlating the Solvating Power of Solvents with the Strength of Ion-Dipole Interaction in Electrolytes of Lithium-ion Batteries, *Angew. Chem., Int. Ed.*, 2023, **62**, e202312373.
8 Z. Piao, R. Gao, Y. Liu, G. Zhou and H.-M. Cheng, A Review on Regulating Li$^+$ Solvation Structures in Carbonate Electrolytes for Lithium Metal Batteries, *Adv. Mater.*, 2023, **35**, 2206009.
9 J. R. Pliego and J. M. Riveros, The cluster-continuum model for the calculation of the solvation free energy of ionic species, *J. Phys. Chem. A*, 2001, **105**, 7241–7247.
10 J. R. Pliego and J. M. Riveros, Hybrid discrete-continuum solvation methods, *Wiley Interdiscip. Rev.: Comput. Mol. Sci.*, 2020, **10**, e1440.
11 A. von Cresce and K. Xu, Preferential Solvation of Li$^+$ Directs Formation of Interphase on Graphitic Anode, *Electrochem. Solid-State Lett.*, 2011, **14**, A154.

12 X. Bogle, R. Vazquez, S. Greenbaum, A. von Cresce and K. Xu, Understanding Li^+–Solvent Interaction in Nonaqueous Carbonate Electrolytes with ^{17}O NMR, *J. Phys. Chem. Lett.*, 2013, **4**, 1664–1668.

13 M. G. Giorgini, K. Futamatagawa, H. Torii, M. Musso and S. Cerini, Solvation Structure around the Li^+ Ion in Mixed Cyclic/Linear Carbonate Solutions Unveiled by the Raman Noncoincidence Effect, *J. Phys. Chem. Lett.*, 2015, **6**, 3296–3302.

14 D. M. Seo, S. Reininger, M. Kutcher, K. Redmond, W. B. Euler and B. L. Lucht, Role of Mixed Solvation and Ion Pairing in the Solution Structure of Lithium Ion Battery Electrolytes, *J. Phys. Chem. C*, 2015, **119**, 14038–14046.

15 K. D. Fulfer and D. G. Kuroda, Solvation Structure and Dynamics of the Lithium Ion in Organic Carbonate-Based Electrolytes: A Time-Dependent Infrared Spectroscopy Study, *J. Phys. Chem. C*, 2016, **120**, 24011–24022.

16 N. Chapman, O. Borodin, T. Yoon, C. C. Nguyen and B. L. Lucht, Spectroscopic and Density Functional Theory Characterization of Common Lithium Salt Solvates in Carbonate Electrolytes for Lithium Batteries, *J. Phys. Chem. C*, 2017, **121**, 2135–2148.

17 K. D. Fulfer and D. G. Kuroda, A comparison of the solvation structure and dynamics of the lithium ion in linear organic carbonates with different alkyl chain lengths, *Phys. Chem. Chem. Phys.*, 2017, **19**, 25140–25150.

18 H. Jiang, Q. Zhang, Y. Zhang, L. Sui, G. Wu, K. Yuan and X. Yang, Li-Ion solvation in propylene carbonate electrolytes determined by molecular rotational measurements, *Phys. Chem. Chem. Phys.*, 2019, **21**, 10417–10422.

19 C. Lim, J. H. Kim, Y. Chae, K.-K. Lee, K. Kwak and M. Cho, Solvation Structure around Li^+ Ions in Organic Carbonate Electrolytes: Spacer-Free Thin Cell IR Spectroscopy, *Anal. Chem.*, 2021, **93**, 12594–12601.

20 I. Skarmoutsos, V. Ponnuchamy, V. Vetere and S. Mossa, Li^+ Solvation in Pure, Binary, and Ternary Mixtures of Organic Carbonate Electrolytes, *J. Phys. Chem. C*, 2015, **119**, 4502–4515.

21 O. Borodin, M. Olguin, P. Ganesh, P. R. C. Kent, J. L. Allen and W. A. Henderson, Competitive lithium solvation of linear and cyclic carbonates from quantum chemistry, *Phys. Chem. Chem. Phys.*, 2016, **18**, 164–175.

22 W. Cui, Y. Lansac, H. Lee, S.-T. Hong and Y. H. Jang, Lithium ion solvation by ethylene carbonates in lithium-ion battery electrolytes, revisited by density functional theory with the hybrid solvation model and free energy correction in solution, *Phys. Chem. Chem. Phys.*, 2016, **18**, 23607–23612.

23 M. Shakourian-Fard, G. Kamath and S. K. R. S. Sankaranarayanan, Evaluating the Free Energies of Solvation and Electronic Structures of Lithium-Ion Battery Electrolytes, *ChemPhysChem*, 2016, **17**, 2916–2930.

24 T. P. Pollard and T. L. Beck, Structure and polarization near the Li^+ ion in ethylene and propylene carbonates, *J. Chem. Phys.*, 2017, **147**, 161710.

25 S. Han, Structure and dynamics in the lithium solvation shell of nonaqueous electrolytes, *Sci. Rep.*, 2019, **9**, 5555.

26 N. Yao, X. Chen, Z.-H. Fu and Q. Zhang, Applying Classical, Ab Initio, and Machine-Learning Molecular Dynamics Simulations to the Liquid Electrolyte for Rechargeable Batteries, *Chem. Rev.*, 2022, **122**, 10970–11021.

27 H. Lee, S. Hwang, M. Kim, K. Kwak, J. Lee, Y.-K. Han and H. Lee, Why Does Dimethyl Carbonate Dissociate Li Salt Better Than Other Linear Carbonates? Critical Role of Polar Conformers, *J. Phys. Chem. Lett.*, 2020, **11**, 10382–10387.

28 B. Koo, H. Lee, S. Hwang, J. Lee, Y.-K. Han, K. H. Ahn, C. Lee and H. Lee, Role of Solvent Isomerism in Mixed Carbonate Electrolytes for Li-Ion Batteries, *J. Phys. Chem. C*, 2023, **127**, 18271–18278.

29 D. Itkis, L. Cavallo, L. V. Yashina and Y. Minenkov, Ambiguities in solvation free energies from cluster-continuum quasichemical theory: lithium cation in protic and aprotic solvents, *Phys. Chem. Chem. Phys.*, 2021, **23**, 16077–16088.

30 A. A. Otlyotov and Y. Minenkov, Conformational energies of microsolvated Na^+ clusters with protic and aprotic solvents from GFNn-xTB methods, *J. Comput. Chem.*, 2022, **43**, 1856–1863.

31 A. A. Otlyotov, D. Itkis, L. V. Yashina, L. Cavallo and Y. Minenkov, Physical and numerical aspects of sodium ion solvation free energies *via* the cluster-continuum model, *Phys. Chem. Chem. Phys.*, 2022, **24**, 29927–29939.

32 A. A. Otlyotov, L. Cavallo and Y. Minenkov, Cluster-Continuum Model as a Sanity Check of Sodium Ions' Gibbs Free Energies of Transfer, *Inorg. Chem.*, 2022, **61**, 18365–18379.

33 M. Bursch, J.-M. Mewes, A. Hansen and S. Grimme, Best-Practice DFT Protocols for Basic Molecular Computational Chemistry, *Angew. Chem., Int. Ed.*, 2022, **61**, e202205735.

34 L. H. Hess and A. Balducci, 1,2-butylene carbonate as solvent for EDLCs, *Electrochim. Acta*, 2018, **281**, 437–444.

35 B. Mosallanejad, S. Sadeghi Malek, M. Ershadi, H. Sharifi, A. Ahmadi Daryakenari, F. Boorboor Ajdari and S. Ramakrishna, Insights into the efficient roles of solid electrolyte interphase derived from vinylene carbonate additive in rechargeable batteries, *J. Electroanal. Chem.*, 2022, **909**, 116126.

36 S. Grimme, Supramolecular binding thermodynamics by dispersion-corrected density functional theory, *Chem. – Eur. J.*, 2012, **18**, 9955–9964.

37 P. Pracht and S. Grimme, Calculation of absolute molecular entropies and heat capacities made simple, *Chem. Sci.*, 2021, **12**, 6551–6568.

38 A. A. Otlyotov and Y. Minenkov, Gas-phase thermochemistry of noncovalent ligand–alkali metal ion clusters: An impact of low frequencies, *J. Comput. Chem.*, 2023, **44**, 1807–1816.

39 S. Miertuš, E. Scrocco and J. Tomasi, Electrostatic interaction of a solute with a continuum. A direct utilizaion of AB initio molecular potentials for the prevision of solvent effects, *Chem. Phys.*, 1981, **55**, 117–129.

40 V. Barone and M. Cossi, Quantum Calculation of Molecular Energies and Energy Gradients in Solution by a Conductor Solvent Model, *J. Phys. Chem. A*, 1998, **102**, 1995–2001.

41 B. Mennucci, Polarizable continuum model, *Wiley Interdiscip. Rev.: Comput. Mol. Sci.*, 2012, **2**, 386–404.

42 Y. Minenkov, Solv: An Alternative Continuum Model Implementation Based on Fixed Atomic Charges, Scaled Particle Theory, and the Atom–Atom Potential Method, *J. Chem. Theory Comput.*, 2023, **19**, 5221–5230.
43 A. K. Rappé, C. J. Casewit, K. S. Colwell, W. A. Goddard and W. M. Skiff, UFF, a Full Periodic Table Force Field for Molecular Mechanics and Molecular Dynamics Simulations, *J. Am. Chem. Soc.*, 1992, **114**, 10024–10035.
44 C. Bannwarth, S. Ehlert and S. Grimme, GFN2-xTB – An Accurate and Broadly Parametrized Self-Consistent Tight-Binding Quantum Chemical Method with Multipole Electrostatics and Density-Dependent Dispersion Contributions, *J. Chem. Theory Comput.*, 2019, **15**, 1652–1671.
45 P. Pracht, F. Bohle and S. Grimme, Automated exploration of the low-energy chemical space with fast quantum chemical methods, *Phys. Chem. Chem. Phys.*, 2020, **22**, 7169–7192.
46 P. Pracht, S. Grimme, C. Bannwarth, F. Bohle, S. Ehlert, G. Feldmann, J. Gorges, M. Müller, T. Neudecker, C. Plett, S. Spicher, P. Steinbach, P. A. Wesołowski and F. Zeller, CREST—A program for the exploration of low-energy molecular chemical space, *J. Chem. Phys.*, 2024, **160**, 114110.
47 GitHub – charnley/rmsd: Calculate Root-mean-square deviation (RMSD) of two molecules, using rotation, in xyz or pdb format, **https://github.com/charnley/rmsd**, (accessed June 6, 2024).
48 W. Kabsch, A solution for the best rotation to relate two sets of vectors, *Acta Crystallogr., Sect. A: Cryst. Phys., Diffr., Theor. Gen. Crystallogr.*, 1976, **32**, 922–923.
49 M. W. Walker, L. Shao and R. A. Volz, Estimating 3-D location parameters using dual number quaternions, *CVGIP Image Underst.*, 1991, **54**, 358–367.
50 J. P. Perdew, K. Burke and M. Ernzerhof, Generalized gradient approximation made simple, *Phys. Rev. Lett.*, 1996, **77**, 3865–3868.
51 J. P. Perdew, K. Burke and M. Ernzerhof, Erratum: Generalized gradient approximation made simple (Physical Review Letters (1996) 77 (3865)), *Phys. Rev. Lett.*, 1997, **78**, 1396.
52 S. Grimme, J. Antony, S. Ehrlich and H. Krieg, A consistent and accurate ab initio parametrization of density functional dispersion correction (DFT-D) for the 94 elements H-Pu, *J. Chem. Phys.*, 2010, **132**, 154104–154119.
53 S. Grimme, S. Ehrlich and L. Goerigk, Effect of the damping function in dispersion corrected density functional theory, *J. Comput. Chem.*, 2011, **32**, 1456–1465.
54 F. Weigend and R. Ahlrichs, Balanced basis sets of split valence, triple zeta valence and quadruple zeta valence quality for H to Rn: Design and assessment of accuracy, *Phys. Chem. Chem. Phys.*, 2005, **7**, 3297–3305.
55 F. Weigend, Accurate Coulomb-fitting basis sets for H to Rn, *Phys. Chem. Chem. Phys.*, 2006, **8**, 1057–1065.
56 J. L. Whitten, Coulombic potential energy integrals and approximations, *J. Chem. Phys.*, 1973, **58**, 4496–4501.
57 E. J. Baerends, D. E. Ellis and P. Ros, Self-consistent molecular Hartree—Fock—Slater calculations I. The computational procedure, *Chem. Phys.*, 1973, **2**, 41–51.
58 B. I. Dunlap, J. W. D. Connolly and J. R. Sabin, On some approximations in applications of Xα theory, *J. Chem. Phys.*, 1979, **71**, 3396–3402.
59 F. Neese, The ORCA program system, *Wiley Interdiscip. Rev.: Comput. Mol. Sci.*, 2012, **2**, 73–78.
60 F. Neese, F. Wennmohs, U. Becker and C. Riplinger, The ORCA quantum chemistry program package, *J. Chem. Phys.*, 2020, **152**, 224108.
61 F. Neese, Software update: The ORCA program system—Version 5.0, *Wiley Interdiscip. Rev.: Comput. Mol. Sci.*, 2022, **12**, e1606.
62 D. Bakowies and O. A. Von Lilienfeld, Density Functional Geometries and Zero-Point Energies in Ab Initio Thermochemical Treatments of Compounds with First-Row Atoms (H, C, N, O, F), *J. Chem. Theory Comput.*, 2021, **17**, 4872–4890.
63 S. Grimme, Improved second-order Møller–Plesset perturbation theory by separate scaling of parallel- and antiparallel-spin pair correlation energies, *J. Chem. Phys.*, 2003, **118**, 9095–9102.
64 D. Feller, K. A. Peterson and J. Grant Hill, On the effectiveness of CCSD(T) complete basis set extrapolations for atomization energies, *J. Chem. Phys.*, 2011, **135**, 044102.
65 Y. Minenkov, L. Cavallo and K. A. Peterson, Influence of the complete basis set approximation, tight weighted-core, and diffuse functions on the DLPNO-CCSD(T1) atomization energies of neutral H,C,O-compounds, *J. Comput. Chem.*, 2023, **44**, 687–696.
66 J. M. L. Martin, *Ab initio* total atomization energies of small molecules – Towards the basis set limit, *Chem. Phys. Lett.*, 1996, **259**, 669–678.
67 A. Hellweg, C. Hättig, S. Höfener and W. Klopper, Optimized accurate auxiliary basis sets for RI-MP2 and RI-CC2 calculations for the atoms Rb to Rn, *Theor. Chem. Acc.*, 2007, **117**, 587–597.
68 J. W. Furness, A. D. Kaplan, J. Ning, J. P. Perdew and J. Sun, Accurate and Numerically Efficient r^2SCAN Meta-Generalized Gradient Approximation, *J. Phys. Chem. Lett.*, 2020, **11**, 8208–8215.
69 J. W. Furness, A. D. Kaplan, J. Ning, J. P. Perdew and J. Sun, Correction to ''Accurate and Numerically Efficient r^2SCAN Meta-Generalized Gradient Approximation'', *J. Phys. Chem. Lett.*, 2020, **11**, 9248.
70 S. H. Vosko, L. Wilk and M. Nusair, Accurate spin-dependent electron liquid correlation energies for local spin density calculations: a critical analysis, *Can. J. Phys.*, 1980, **58**, 1200–1211.
71 C. T. Lee, W. T. Yang and R. G. Parr, Development of the Colle-Salvetti correlation-energy formula into a functional of the electron density, *Phys. Rev. B*, 1988, **37**, 785–789.
72 A. D. Becke, Density-functional thermochemistry. III. The role of exact exchange, *J. Chem. Phys.*, 1993, **98**, 5648–5652.
73 C. Adamo and V. Barone, Toward reliable density functional methods without adjustable parameters: The PBE0 model, *J. Chem. Phys.*, 1999, **110**, 6158–6170.
74 E. Caldeweyher, C. Bannwarth and S. Grimme, Extension of the D3 dispersion coefficient model, *J. Chem. Phys.*, 2017, **147**, 34112.

75 E. Caldeweyher, S. Ehlert, A. Hansen, H. Neugebauer, S. Spicher, C. Bannwarth and S. Grimme, A generally applicable atomic-charge dependent London dispersion correction, *J. Chem. Phys.*, 2019, **150**, 154122.
76 N. Mardirossian and M. Head-Gordon, ωB97M-V: A combinatorially optimized, range-separated hybrid, meta-GGA density functional with VV10 nonlocal correlation, *J. Chem. Phys.*, 2016, **144**, 214110.
77 O. A. Vydrov and T. Van Voorhis, Nonlocal van der Waals density functional: The simpler the better, *J. Chem. Phys.*, 2010, **133**, 244103.
78 A. Najibi and L. Goerigk, The Nonlocal Kernel in van der Waals Density Functionals as an Additive Correction: An Extensive Analysis with Special Emphasis on the B97M-V and ωB97M-V Approaches, *J. Chem. Theory Comput.*, 2018, **14**, 5725–5738.
79 S. Grimme, J. G. Brandenburg, C. Bannwarth and A. Hansen, Consistent structures and interactions by density functional theory with small atomic orbital basis sets, *J. Chem. Phys.*, 2015, **143**, 54107.
80 J. G. Brandenburg, C. Bannwarth, A. Hansen and S. Grimme, B97-3c: A revised low-cost variant of the B97-D density functional method, *J. Chem. Phys.*, 2018, **148**, 064104.
81 S. Grimme, A. Hansen, S. Ehlert and J.-M. Mewes, r^2SCAN-3c: A "Swiss army knife" composite electronic-structure method, *J. Chem. Phys.*, 2021, **154**, 64103.
82 M. J. S. Dewar, E. G. Zoebisch, E. F. Healy and J. J. P. Stewart, Development and use of quantum mechanical molecular models. 76. AM1: a new general purpose quantum mechanical molecular model, *J. Am. Chem. Soc.*, 1985, **107**, 3902–3909.
83 J. J. P. Stewart, Optimization of parameters for semiempirical methods I. Method, *J. Comput. Chem.*, 1989, **10**, 209–220.
84 J. J. P. Stewart, Optimization of parameters for semiempirical methods V: Modification of NDDO approximations and application to 70 elements, *J. Mol. Model.*, 2007, **13**, 1173–1213.
85 J. Řezáč and P. Hobza, Advanced Corrections of Hydrogen Bonding and Dispersion for Semiempirical Quantum Mechanical Methods, *J. Chem. Theory Comput.*, 2012, **8**, 141–151.
86 J. J. P. Stewart, Optimization of parameters for semiempirical methods VI: More modifications to the NDDO approximations and re-optimization of parameters, *J. Mol. Model.*, 2013, **19**, 1–32.
87 S. Grimme, C. Bannwarth and P. Shushkov, A Robust and Accurate Tight-Binding Quantum Chemical Method for Structures, Vibrational Frequencies, and Noncovalent Interactions of Large Molecular Systems Parametrized for All spd-Block Elements (Z = 1–86), *J. Chem. Theory Comput.*, 2017, **13**, 1989–2009.
88 D. N. Laikov, A new parametrizable model of molecular electronic structure, *J. Chem. Phys.*, 2011, **135**, 134120.
89 K. R. Briling, Comment on "A new parametrizable model of molecular electronic structure" [J. Chem. Phys. 135, 134120 (2011)], *J. Chem. Phys.*, 2017, **147**, 157101.
90 D. N. Laikov and Y. A. Ustynyuk, PRIRODA-04: A quantum-chemical program suite. New possibilities in the study of molecular systems with the application of parallel computing, *Russ. Chem. Bull.*, 2005, **54**, 820–826.
91 J. J. P. Stewart, MOPAC2016; Stewart Computational Chemistry: Colorado Springs, CO, USA, 2016. **https://openmopac.net** (accessed July 30, 2024).
92 C. Bannwarth, E. Caldeweyher, S. Ehlert, A. Hansen, P. Pracht, J. Seibert, S. Spicher and S. Grimme, Extended tight-binding quantum chemistry methods, *Wiley Interdiscip. Rev.: Comput. Mol. Sci.*, 2021, **11**, e1493.
93 S. F. Vyboishchikov and A. A. Voityuk, Fast non-iterative calculation of solvation energies for water and non-aqueous solvents, *J. Comput. Chem.*, 2021, **42**, 1184–1194.
94 A. V. Marenich, S. V. Jerome, C. J. Cramer and D. G. Truhlar, Charge Model 5: An Extension of Hirshfeld Population Analysis for the Accurate Description of Molecular Interactions in Gaseous and Condensed Phases, *J. Chem. Theory Comput.*, 2012, **8**, 527–541.
95 K. Duanmu and D. G. Truhlar, Partial Ionic Character beyond the Pauling Paradigm: Metal Nanoparticles, *J. Phys. Chem. C*, 2014, **118**, 28069–28074.
96 K. Duanmu, B. Wang, A. V. Marenich, C. J. Cramer and D. G. Truhlar, *CM5PAC Version*, 2015.
97 Y. Kameda, S. Saito, Y. Umebayashi, K. Fujii, Y. Amo and T. Usuki, Local structure of Li^+ in concentrated $LiPF_6$–dimethyl carbonate solutions, *J. Mol. Liq.*, 2016, **217**, 17–22.
98 B. P. Kar, N. Ramanathan, K. Sundararajan and K. S. Viswanathan, Matrix isolation and DFT study of the conformations of diethylcarbonate, *J. Mol. Struct.*, 2014, **1072**, 61–68.

